
Physical conditions of the shocked regions in collimated outflows of planetary nebulae

A. Riera¹ and A.C. Raga²

¹ Departament de Física i Enginyeria Nuclear. EUETIB. Universitat Politècnica de Catalunya. Compte d’Urgell 187, E-08036 Barcelona, Spain.

`angels.riera@upc.edu`

² Instituto de Ciencias Nucleares. Universidad Nacional Autónoma de México, Ap. 70-543, 04510 D.F., México. `raga@nucleares.unam.mx`

Summary. We review the physical properties of the high-velocity pairs of knots and jets observed in planetary nebulae. We address the need of identifying the observational properties of the “irradiated shocks” (i.e. bow shocks irradiated by the central star). We characterize the spectra of several bow shock-like structures (or FLIERs) from ground-based spectroscopical data and narrowband WFPC2 HST images. We present first results of axisymmetric simulations of initially ionized, dense cloudlets which move away from the exciting source, taking into consideration the effect of the ionizing radiation field. We obtain predicted line ratios for the irradiated bow shocks which can be compared directly with the observations of FLIERs. We find a reasonable agreement which can be seen as a confirmation of the interpretation of FLIERs as “irradiated shocks”.

Key words: planetary nebulae: general. ISM: jets and outflows.

1 Introduction

The existence of small-scale structures in planetary nebulae (PNe) has been known since the pioneering work of [1]. Since then, the subsequent spectroscopic studies have shown that these structures differ significantly from their surroundings in either line ratios or radial velocities or both. Of particular interest are the strings of knots appearing as symmetrical pairs, point-symmetrical features or jet structures, which move supersonically with respect to the main body of the nebula. Here we use the term FLIERs (Fast Low Ionization Emission Region) introduced by Balick and coworkers to describe those structures. The morphologies and dynamics of FLIERs suggest that PN nuclei intermittently eject highly collimated outflows or clumps ([3], [4]). As a result of the interaction of the clumps or collimated outflows with the surrounding gas, bow shocks are expected to form. See the reviews by [14], [15], and [9] for a description of the observational properties of collimated outflows in PNe.

2 Physical conditions and excitation of FLIERS

Balick and coworkers explored the spectroscopic properties of FLIERS in a group of PNe (reported in a series of four papers: [3],[4],[11], and [5]). Recently, Goncalves et al. enlarged the sample of observed objects ([9], [10]). Those authors found that FLIERS have dimensions of $\sim 10^{16}$ cm, are much lower in ionization, higher in velocity (with doppler shifts of $\pm 25\text{--}200$ km s $^{-1}$) and about the same in density and temperature compared with the regions around them. A rather surprising result of the ground-based studies is that the physical conditions (electron density and temperature) are, in most cases, much the same within the high-velocity knots and jets and in the surrounding nebula (see Goncalves, these proceedings). However, the electron densities could be larger than the values derived from [S II] line ratio if the [S II] lines are affected by collisional quenching ([19]). On the other hand, the use of ground-based spectroscopy presents serious drawbacks, such as the difficulty in untangling the intrinsic spectrum of the FLIER from the adjacent nebula, and to spatially resolve its density structure. The use of the WFPC2 onboard HST revealed that many FLIERS show an ionization stratification, with the gas in the downstream region being more highly ionized than the leading (outward-facing) edge ([5]).

There are few PNe with knots or bow shock-like structures whose spectra can be explained in terms of pure shocks, such as K 4–47 ([8]), M 2–48 ([25], [17]), IC 4593 (Goncalves these proceedings), and KjPn8 ([16]). In these objects, the electron temperatures of the knots are well above 16000 K (as expected for a shock-excited gas). The electron densities derived from the bright [S II] lines range from 100 cm $^{-3}$ (M 2–48) up to a few times 10 3 cm $^{-3}$ (as in the knots of K 4–47 and IC 4593). Comparisons of the spectra of the knots of these PNe with the predictions of either plane-parallel or simple bow-shock models widely applied to HH objects, reveals that the observed emission is mainly shock excited with an intermediate (M 2–48) or large (K 4–47, KjPn8) shock velocities ([17], [8], [16]).

With the exception of the group of PNe mentioned above, simple bow-shock models (i.e. “pure” shocks) fail to reproduce some of the observed properties of FLIERS, such as the observed gradient of ionization, the detailed values of the emission line ratios and the lack of electron density and temperature contrast between the FLIER and the surrounding nebula (see [5] and [23] for a detailed discussion of the caveats of the bow shock models). Even so, the small sizes and high outflowing velocities of the FLIERS strongly support that these microstructures are associated to outward-flowing bullets or clumps. Consequently, the emission observed at the FLIERS would form in a bow shock which is irradiated by the central star (i.e. the central star is an ionizing photon source that will modify the ionization and excitation structure of the shock). We refer to these shocks as irradiated shocks.

2.1 Characterization of irradiated shocks in PNe

In order to characterize the spectra of the irradiated shocks we have chosen three nebulae (NGC 6543, NGC 7009 and IC 4634) which have bow-shock like features outside the main body of the nebula and for which images of several emission lines have been obtained with the WFPC2 onboard HST³. We have obtained image ratios of several regions at every pixel with surface brightness above a threshold value of 3σ . The resulting $[\text{O III}]/\text{H}\alpha$ and $[\text{N II}]/\text{H}\alpha$ ratio maps of the outer bow-shock of IC 4634 (Guerrero et al. in preparation), the northern jet of NGC 6543 [2] and the western outer FLIER of NGC 7009 [5] are shown in Figure 1.

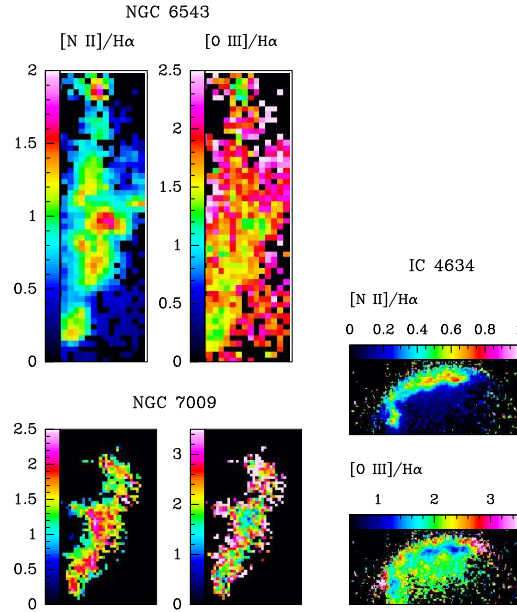


Fig. 1. $[\text{O III}] 5007/\text{H}\alpha$ and $[\text{N II}] 6543/\text{H}\alpha$ ratio maps of a FLIER for each PNe (see the text).

Of particular interest is the small-scale structure of the outer bow-shocks of IC 4634, which shows abrupt changes in these emission line ratios (as illustrated in Figure 1). Behind the bow-shock structures, $[\text{O III}]$ is enhanced, with $[\text{O III}]/\text{H}\alpha$ values from 2 to 3. In the brightest regions (i.e. in the emitting knots of these features) the $[\text{O III}]/\text{H}\alpha$ ratio declines to 1 – 1.5, while the $[\text{N II}]$ emission is greatly enhanced. Note the enhancement of the $[\text{O III}]/\text{H}\alpha$ ratio in cap-like structures just outside the bow-shock plotted in Figure 1 (the

³ The reduced HST images of NGC 6543 and NGC 7009 were kindly provided by Dr. Balick.

presence of a skin of enhanced $[\text{O III}]/\text{H}\alpha$ ratio in PNe is discussed in Medina et al. in these proceedings). The knots within the western outer FLIER of NGC 7009 are characterized by large $[\text{N II}]/\text{H}\alpha$ values (from 1.5 to 2.5) and $[\text{O III}]/\text{H}\alpha$ ratios $\sim 1-2$. The latter ratio increases behind the bow shock (i.e. at the edge facing towards the central source), following the ionization stratification also found in the outer bow-shocks of IC 4634 among other cases. The knots of the northern jet of NGC 6543 are characterized by $[\text{O III}]/\text{H}\alpha \sim 1.5$ and $[\text{N II}]/\text{H}\alpha \sim 1 - 1.5$. The knots are embedded in a diffuse gas which shows larger $[\text{O III}]/\text{H}\alpha$ (≥ 2) and lower $[\text{N II}]/\text{H}\alpha$ (~ 0.5) ratios than the corresponding values within the knots.

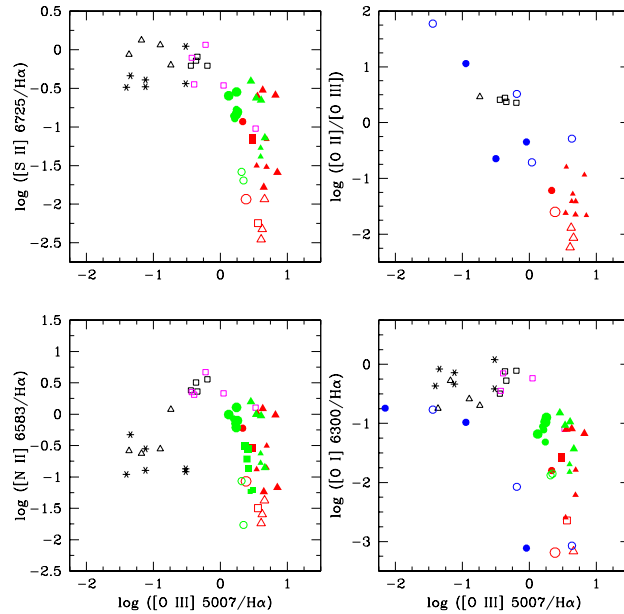


Fig. 2. Diagnostic diagrams including several de-reddened emission line ratios. Black symbols: PPNe (squares: Hen 3-1475 ([20], [21]), triangles: M 1-92, M 2-56 and OH 238.1+4.2 ([24], [22]), stars: CRL 618 (Riera et al. in prep.)). Magenta squares: knots of K 4-47 and M 2-48 ([8], [17]). Red symbols correspond to ground-based spectroscopical data of NGC 6543 (circles), NGC 7009 (triangles) and IC 4634 (squares) are taken from [4], [6], and Guerrero et al. (in preparation). Green symbols: synthesized spectra of different regions of NGC 6543, NGC 7009 and IC 4634 obtained from the WFPC2 HST images ([13] and this work). Filled symbols correspond to FLIERs, open symbols correspond to rims and shells. Blue dots: synthesized spectra obtained from the predicted emission line maps (see Sect. 3).

In Figure 2 we present a set of diagnostic diagrams, involving several emission line ratios, commonly used to discriminate photoionized nebulae from shock-excited objects. The sample of proto-PNe defines the region of (pure)

shocked objects. We have included ground-based spectroscopical data and the spectra synthesized from the WFPC2 HST images of different regions of NGC 6543, NGC 7009 and IC 4634. Open symbols correspond to rims and shells and have been included to trace the locus of photoionized gas. The irradiated shocks (i.e. FLIERs) are plotted as red (ground-based spectroscopical data) and green (values obtained from WFPC2 HST narrowband images) filled symbols of various forms. The size of the symbol is an indication of the distance from the feature to the central star; larger symbols represent features at larger distances from the star. The ratio of $[\text{O III}]/\text{H}\alpha$ alone discriminates the shocked objects from the rest, but there is a considerable overlap between photoionized gas and irradiated shocks ($[\text{O III}]/\text{H}\alpha = 1.5$ to 6). Different features of our sample of PNe define a sequence in the diagrams of figure 2. The photoionized regions occupy the high ionization end of this sequence (i.e. the region with the lowest values of $[\text{N II}]/\text{H}\alpha$, $[\text{S II}]/\text{H}\alpha$ and $[\text{O I}]/\text{H}\alpha$). We conclude that the spatially integrated emission of irradiated shocks are characterized by a considerable range in $[\text{N II}]/\text{H}\alpha$, $[\text{S II}]/\text{H}\alpha$ and $[\text{O I}]/\text{H}\alpha$ emission line ratios, with values between the expected values for pure shock-excited objects and photoionized nebulae. The 2D images of the irradiated shocks are characterized by the spatial ionization stratification described above and the presence of large variations in the excitation conditions on small scales.

3 Numerical simulations of irradiated shocks

We carried out a 2D, axisymmetric gasdynamical simulations of a high velocity cloudlet that moves away from the central star through the photoionized, nebular gas. We use a time-dependent gasdynamic code (with an adaptative grid) that includes radiative, dielectronic and charge exchange recombinations, collisional ionization and photoionization for several species (described in [18]). We include the radiation field from the central star that penetrates the recombination region behind the leading bow shock from "behind" (i.e., in the direction from the post-shock to the pre-shock region). We have chosen an initial clump density of 10^3 cm^{-3} , an initial temperature 10^4 K , and a clump radius of 10^{16} cm . The clump is initially fully ionized (i.e., $\text{H}^+/\text{H} = 1$, $\text{He}^+/\text{He} = 1$) and moves at a velocity of 100 km s^{-1} with respect to the environmental gas. The environmental gas has a density of 100 cm^{-3} , a temperature of 10^4 K , and is fully (singly) ionized. The star has a blackbody spectrum with an effective temperature of 50000 K and a luminosity of $5000 L_{\odot}$. The abundances are mean PN abundances taken from [12]. We obtain three simulations with initial distances from the cloudlet to the star of $3 \cdot 10^{18} \text{ cm}$ (model M1), 10^{18} cm (M2) and $3 \cdot 10^{17} \text{ cm}$ (M3). Models M1-M3 have been computed in order to explore the effect of the ionizing photon flux as a function of the local ionizing parameter (U), which increases from $U = 10^{-5}$ (M1) to $U = 10^{-3}$ (M3).

3.1 Model results

Figure 3 illustrates the density stratification and the H neutral fraction distribution as a function of time for model M2 ($U=10^{-4}$). This figure illustrates how the cloudlet fragments. The motion of a cloudlet through a medium induces a “cloudlet shock” that compresses the bullet and provokes its fragmentation.

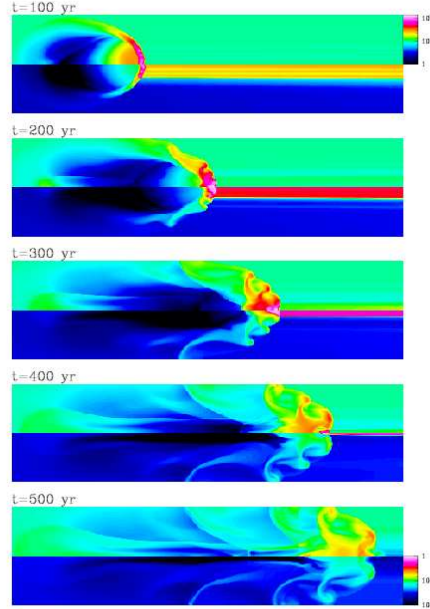


Fig. 3. Density (top half of each plot) and neutral fraction of H (bottom half) obtained for $t=100, 200, 300, 400, 500$ yr integration times from model M2. The logarithmic density stratification is given (in cm^{-3}) by the bar on the top right, and the logarithmic hydrogen neutral fraction stratification is given by the bottom right bar.

In model M1 (with $U = 10^{-5}$) the high density gas within the bow-shock traps an ionization front. For model M3 (with $U = 10^{-3}$) the impinging photon flux is strong enough to fully ionize the high density material. As a consequence the bow shock remains partially neutral for M1 while for M2 and M3 the high density gas becomes almost fully ionized. A comparison of the density stratification for the three models reveals a more complex density structure as U decreases. This appears to be the result of the higher compression of the gas as it cools to temperatures well below 10^4 K in the low U models.

3.2 Comparison with the observations

We have computed the emission maps of the $H\alpha$, [O I] 6300, [O II] 3727, and [O III] 5007 lines, which span a range of ionization energies, for the three models and for a $t=200$ years integration time. The model of the lowest U shows extended emission in [O II], and the [O III] map shows a complete absence of emission at the tip of the bow-shock and a very low intensity at the wings. On the other hand, the [O I] emission is mainly arising from the tip of the bow-shock. As the photon flux reaching the bow-shock increases the [O III] intensity increases. The predicted [O III]/ $H\alpha$ map qualitatively reproduces the observed increase of this emission line ratio behind the bow-shock. For models M2 and M3 the [O III]/ $H\alpha$ ratio show values ~ 3 in good agreement with the observations (see Sect. 2).

In order to quantify the agreement between the observed and predicted spectra we have obtained the spatially integrated spectra of the irradiated bow-shock for models M1–M3 and plotted the results in the diagnostic diagrams of Figure 2). Model M1 (low U , kinetic-dominated shock) approximately reproduces the spectral characteristics of the shock-excited nebulae, while model M3 (high U , photon-dominated shock) fits the spectra of the photoionized regions of the PNe. Models with intermediate U values reproduce the expected values for an irradiated shock at various distances from the central source, with the exception of the [O III]/ $H\alpha$ line ratio. The most important difference between the predictions and observations is that the predicted [O III]/ $H\alpha$ ratios are lower than the observed ones by a factor of 5. Higher [O III] emission could be obtained from models with a higher effective temperature for the photoionizing spectrum. However, such models have not been explored in the present work.

4 Conclusions

We conclude that the spatially integrated spectra of FLIERs are characterized by strong low excitation emission lines (relative to $H\alpha$) which become fainter as the FLIER approaches to the central source. The high excitation, [O III] line (relative to $H\alpha$) has similar values in FLIERs and photoionized nebula. First results of axisymmetric simulations of initially ionized, dense cloudlets which move away from the exciting source, taking into consideration the effect of the ionizing radiation field, qualitatively reproduces the spatial ionization stratification observed in FLIERs. The predicted emission line ratios approximately reproduces the spectra observed in FLIERs. The most important difference between the predictions and observations is that the predicted [O III]/ $H\alpha$ ratios are lower than the observed ones. Higher [O III] emission could be obtained from models with a higher effective temperature for the photoionizing spectrum. In a future work we will study the effect of increasing the temperature of the central star and the velocity of the cloudlet.

References

1. L. W. Aller: *ApJ* **93**, 236 (1941)
2. B. Balick: *AJ*, **127**, 2262 (2004)
3. B. Balick, M. Rugers, Y. Terzian, J.N. Chengalur: *ApJ*, **411**, 778 (1993)
4. B. Balick, M. Perinotto, A. Maccioni, Y. Terzian, A. Hajian: *ApJ*, **424**, 800 (1994)
5. B. Balick, J. Alexander, A.R. Hajian, Y. Terzian, M. Perinotto, P. Patriarchi: *AJ*, **116**, 360 (1998)
6. D.R. Goncalves, R.L.M. Corradi, A. Mampaso: *ApJ*, **547**, 302 (2001)
7. D.R. Goncalves, R.L.M. Corradi, A. Mampaso, M. Perinotto: *ApJ*, **597**, 975 (2003)
8. D.R. Goncalves, A. Mampaso, R.L.M. Corradi, M. Perinotto, A. Riera, L. López-Martín: *MNRAS*, **355**, 37 (2004)
9. D.R. Goncalves: Characterizing Low-Ionization Structures in PNe. In: *ASP Conference Proceedings*, vol. 313, ed by M. Meixner, J.H. Kastner, B. Balick and N. Soker (San Francisco: Astronomical Society of the Pacific 2004) pp 216–223
10. D.R. Goncalves, A. Mampaso, R.M.L. Corradi, M. Perinotto: The physical parameters and excitation of jets and knots in PNe. In: *ASP Conference Proceedings*, vol. 313, ed by M. Meixner, J.H. Kastner, B. Balick and N. Soker (San Francisco: Astronomical Society of the Pacific 2004) pp 198–202
11. A. Hajian, B. Balick, Y. Terzian, M. Perinotto: *ApJ*, **487**, 304 (1997)
12. R.L. Kingsburgh, M.J. Barlow: *MNRAS*, **271**, 257 (1994)
13. N.J. Lamé, J.P. Harrington, K. Borkowski: Physical conditions in NGC 6543. In: *Planetary nebulae, Proceedings of the 180th Symposium of the IAU*, ed. by H. J. Habing and H. J. G. L. M. Lamers (Dordrecht: Kluwer Academic Publishers), p.252 (1997)
14. J.A. López: Collimated Outflows in Planetary Nebulae. In: *RMxAA (Serie de Conferencias)*, vol. 9, ed by J. Arthur, N. Brickhouse, J. Franco (2000), pp 102–209
15. J.A. López: Emission Lines from Jets in Planetary Nebulae. In: *RMxAA (Serie de Conferencias)*, vol. 13, ed by W. J. Henney, W. Steffen, A. C. Raga, and L. Binette (2002), pp 139–144
16. J.A. López, R. Vázquez, L.F. Rodríguez: *ApJ Letters*, **L63–L66** (1995)
17. L. López-Martín, J.A. López, C. Esteban, R. Vázquez, A.C. Raga, J.M. Torrelles, L.F. Miranda, J. Meaburn, L. Olguín: *A&A*, **388**, 652 (2002)
18. G. Mellema, A.C. Raga, J. Cantó, P. Lundqvist, B. Balick, W. Steffen, A. Noriega-Crespo: *A&A*, **331**, 335 (1998)
19. M. Perinotto, P. Patriarchi, B. Balick, R.L.M. Corradi: *A&A*, **422**, 963
20. A. Riera, P. García-Lario, A. Manchado, S.R. Pottasch, A.C. Raga: *A&A*, **302**, 137 (1995)
21. A. Riera, L. Binette, A.C. Raga: *A&A*, **455**, 203 (2006)
22. C. Sánchez Contreras, V. Bujarrabal, L.F. Miranda, M.J. Fernández-Figueroa: *A&A*. **357**, 651
23. N. Soker, O. Regev: *AJ*, **116**, 2462 (1998)
24. S.R. Trammell, H.L. Dinerstein, R.W. Goodrich: *ApJ*, **402**, 249 (1993)
25. R. Vázquez, L. López-Martín, L.F. Miranda, C. Esteban, J.M. Torrelles, L. Arias, A.C. Raga: *A&A*, **357**, 1031 (2000)